Chronostratigraphy, depositional patterns and climatic imprints in Lake Acigöl (SW Anatolia) during the Quaternary

François Demory, Claire Rambeau, Anne-Élisabeth Lebatard, Mireille M. Perrin, Syed Blawal, Valérie Andrieu-Ponel, Pierre Rochette, Hülya Alçiçek, Nicolas Boulbes, Didier L. Bourlès, et al.

Chronostratigraphy, depositional patterns and climatic imprints in Lake Acigöl (SW Anatolia) during the Quaternary

François Demory [a,*], Claire Rambeau [b,j], Anne-Elisabeth Lebatard [a], Mireille Perrin [a], Syed Blawal [b], Valérie Andrieu-Ponel [c], Pierre Rochette [a], Hülya Alçiçek [d], Nicolas Boulbes [e], Didier Bourlès [a], Cahit Helvaci [f], Rainer Petschick [g], Serdar Mayda [h], Anne-Marie Moigne [e], Sébastien Nomade [i], Philippe Ponel [c], Amélie Vialet [e], Mehmet Cihat Alçiçek [d], ASTER Team

[a] *Aix Marseille Univ, CNRS, IRD, INRA, Coll France, CEREGE, Aix-en-Provence, France*
[b] *Sedimentology, Albert-Ludwigs-Universität Freiburg, Friedrichstrasse 39, 79098, Freiburg, Germany*
[c] *Institut Méditerranéen de Biodiversité et d'Ecologie Marine et Continentale (IMBE), Aix-Marseille Univ (AMU), Avignon Université, CNRS, IRD, Marseille, OSU Institut Pytheas, Technopôle de l'Environnement Arbois-Méditerranée, BP 80, 13545, Aix-en-Provence Cedex 4, France*
[d] *Pamukkale University, Department of Geology, 20070, Denizli, Turkey*
[e] *Centre Européen de Recherches Préhistoriques de Tautavel, Muséum National d'Histoire Naturelle – UMR 7194, CNRS – Université de Perpignan Via Domitia, Avenue Léon Jean Grégory, 66720, Tautavel, France*
[f] *Dokuz Eylül University Department of Geology, 35160, Izmir, Turkey*
[g] *Goethe-Universität Frankfurt, Institut für Geowissenschaften, Altenhöferallee 1, 60438, Frankfurt am Main, Germany*
[h] *Ege University, Department of Biology, 35100, Izmir, Turkey*
[i] *Laboratoire des Sciences du Climat et de L'Environnement (IPSL-CEA-CNRS-UVSQ), Domaine du CNRS Bât. 12, Avenue de la Terrasse, 91198, Gif Sur Yvette, France*
[j] *Laboratoire Image Ville Environnement (LIVE), University of Strasbourg-CNRS-ENGEES, 3 Rue de l'Argonne, 67083 Strasbourg, France*

ARTICLE INFO

Keywords:
Lake sediment
Turkey
Paleomagnetic dating
Quaternary paleoclimatic records
Paleoenvironmental reconstructions

ABSTRACT

A 601 m long sedimentary sequence was drilled in Lake Acigöl, located in the lakes region of SW Anatolia, near the Denizli travertine from which the oldest hominin of Turkey was unearthed. Among all dating methods applied to the sedimentary sequence, paleomagnetism, through the recognition of geomagnetic chrons, was the most successful and led to a quasi linear age model, with the 601 m long sedimentary record covering the last 2.3 Ma. An attempt to use the atmospherically deposited ^{10}Be as a dating method was not very successful but provides interesting clues on this new method. Long-term lake level changes are depicted through lithological variations, in particular the carbonates and evaporites abundance. This change could be influenced by both long term cooling during the last 2 Ma and tectonic activity, which may in particular be responsible for a maximum water depth at around 1.8 Ma. Despite active tectonic influence, the sedimentary facies description and the magnetic susceptibility record (cleaned from tephra intervals) show that climate fluctuations (i.e., glacial-interglacial alternations) are likely recorded in the sedimentary succession, with warm periods marked by enhanced carbonate precipitation and cold and dry periods characterized by more detrital input linked to reduced vegetation cover and consequently more erosion in the catchment area. Preliminary pollen data, used to interpret magnetic susceptibility fluctuations, show that an average dry and open landscape prevailed around Acigöl lake during the whole record.

1. Introduction

The Acigöl basin is part of a series of fluvio-lacustrine deposits resulting from late Miocene extension processes that affected the lakes domain in SW Anatolia. The conditions of filling were controlled by both lake level variations and active subsidence due to a normal fault located on the basin's southern margin (Price and Scott, 1994; Ten Veen et al., 2009; Alçiçek, 2009; Alçiçek et al., 2013a). Today, particular hydrological conditions induce the presence of a shallow permanent lake filled with magnesium-rich waters that are industrially exploited through evaporation ponds (Alçiçek, 2009; Helvaci et al., 2013).

In the framework of this exploitation, the private company ALKIM

* Corresponding author.
E-mail address: demory@cerege.fr (F. Demory).

https://doi.org/10.1016/j.quageo.2019.101038
Available online 18 November 2019

recovered in 2009, close to the centre of the basin (37°49′35″N, 29°53′27E), a 601 m long core (C3, Fig. 1). Two other cores were extracted by a sister company SODAS (C1-400 m long and C2-150 m long, Fig. 1) in the southwest of Lake Acigöl.

The sedimentary sequence close to the basin centre (C3), potentially the longest continuous continental record in this region, offers a unique opportunity to study the long-term lake level evolution of the basin, past environmental changes, and their coupling during the Quaternary. It is also located along the migratory axis of hominin populations from Africa to Europe and 40 km east of the Kocabaş (Denizli) travertine, from which the remains of the oldest *Homo erectus* of Turkey (Kappelman et al. 2008; Vialet et al. 2012, 2018) have been unearthed. These remains were dated at 1.6–1.2 Ma (Lebatard et al., 2014) and coexist with a rich fauna comprising elephants (*Archidiskodon meridionalis meridionalis*), horses (*Equus cf. altidens s.l.* and *E. cf. apolloniensis*), rhinoceros (*Stephanorhinus cf. etruscus*), small and large-sized deer (*Metacervoceros rhenanus*, *Arvernoceros sp.*, *Cervalces* (*Libralces*), giraffe (*Palaeotragus sp.*), antelope (*Gazella sp.*) and bull (*Bovinae gen. indet*) (Boulbes et al., 2014a, b). The study of Lake Acigöl sediments may therefore help to establish the paleoenvironmental conditions during hominin colonization of Anatolia and migration toward Europe. This will be the subject of a later publication, aimed in particular at describing the plant resources available for hominins using palynology, together with the landscape and climate they lived in. The present publication is mainly devoted to the chronology and general characterization of the sedimentary archive. To depict the paleoenvironmental history recorded in Lake Acigöl sediments, a multidisciplinary approach was applied: i) a combination of dating techniques (magnetostratigraphy and radiochronology) in order to establish an accurate chronological framework; and ii) a combination of geophysical, geochemical, lithological and biological techniques (magnetic susceptibility, carbonate content, facies description, X-ray diffractometry and pollen analysis) to examine the sedimentary history of Lake Acigöl and to determine the respective influences of tectonics, local environmental factors, and/or climate fluctuations.

2. Geological and hydrological setting

Lake Acigöl, formed through progressive narrowing and localized subsidence, is located in a depression surrounded by a Late Miocene sedimentary succession (Price and Scott, 1994; Alçiçek et al., 2013b, 2019) composed of three distinctive units of (1) coarse clastic alluvial-fan deposits, (2) fine-grained and channelized fluvial deposits, and (3) lacustrine deposits with minor evaporatic intercalations. This succession fills the Acıgöl basin (Fig. 1) - a WNW-ESE trending depression 30 km long and 10 km wide - lying on Mesozoic-Paleogene carbonate and ultramafic bedrocks (Göktaş et al., 1989).

The Lake Acıgöl surface and altitude reach at their maximum 156 km^2 and 836 m above sea level, respectively. Level varies due to seasonal dry-up, leading to the development of playa environments. The modern lake is the second largest alkaline lake in the world with active precipitation of sodium, calcium, magnesium and potassium salts. The high salinities in modern Lake Acigöl leading to the dominant precipitation of Mg-rich carbonate and Na-sulfate are linked to a combination of the catchment bedrock and associated groundwater characteristics, topography and seasonal climate with a high evaporation (up to 75.4 cm y^{-1} from open water bodies) to precipitation (ca. 40 cm y^{-1}) ratio (Mutlu et al., 1999; Alçiçek, 2009; Helvaci et al., 2013). Modern climate in the study area is also characterized by extreme temperature variations between seasons (mean daily temperature in January 3.3 °C, and July 24.4 °C) and day and night, all these leading to annual cycles of sediment precipitation and dissolution in the playa. Springs and groundwater in the Acigol basin are generally of moderate salinity and dominated by Ca–Mg– HCO_3 ions in the north and by Na–Ca–SO_4–HCO_3 ions in the south, and their variable input into the lake is one of the major factor controlling the brine composition (Helvaci et al., 2013). Over 30 species of endogenic precipitates and authigenic minerals have been identified in the Acıgöl lacustrine sediments (Helvaci et al., 2013). The most common non-detrital components of the modern sediments include: calcium and calcium-magnesium carbonates (magnesian calcite, aragonite, dolomite), sodium, magnesium, sodium-magnesium sulfates (mirabilite, bloedite, gypsum), and halite. The high Mg/Ca ratios in the basin brines result in hydromagnesite, magnesite, and huntite depositions.

Allogenic input to the lake comprises clay and carbonate minerals, quartz, olivine, pyroxene and feldspars (Helvaci et al., 2013). The detrital fraction may include direct by-products of erosion from the local ultramafic–dolomitic bedrock, but also recycled material from alluvial and former lacustrine sediments that deposited in the Acigöl basin since the late Miocene and are exposed on the edge of Lake Acigöl (Alçiçek, 2009). Detrital carbonate identified in Lake Acigöl sediments by Helvaci et al. (2013) are dolomite and calcite, the former being usually dominant. The outcropping Pliocene lake successions are characterized by extensive dolomitic sediments (Alçiçek, 2009) that are probably partly redeposited in more recent deposits of Lake Acigöl (Helvaci et al., 2013). Agents of transport of allogenic components to the lake include floods, especially for quartz and pyroxene (Helvaci et al., 2013) and aeolian input (average wind speed is moderate to high and mainly from the northeast). Sedimentological, geochemical and mineralogical characteristics of the C3 Acigöl core (e.g. Helvaci et al., 2013) have shown that the lake has evolved through time from deeper and more perennial environments to shallower and more ephemeral environments controlled by the evaporation and precipitation processes.

3. Material and methods

The C3-601 m long core is stored at the site of the ALKIM Company in SW Anatolia, and the C1-400 m long and C2-150 m long cores are stored in the sister company SODAS. 495 subsamples were collected regularly along the C3 core and stored at the CEREGE facility in Aix-en-Provence (France). One sample was also collected from the upper part of the C1 core to estimate the initial authigenic $^{10}Be/^{9}Be$ ratio, as a proxy for the upper part of the C3 core. Actually, the upper 170 m of the C3 core have been soaked with water to sample U-Channels for ITRAX measurements by Akçer-On et al., (2016), and cannot be used anymore for that type of analysis.

3.1. Sedimentology and palynology

A new synthetic lithological profile for Lake Acigöl was established from visual core description and based on the detailed examination of 441 samples. 404 of these samples were separated by less than 2 m, and 314 by less than 1 m. Observations from previous studies of the core (Helvaci et al., 2013) were also taken into account. Sediments were classified according to texture, carbonate contents (visual observations and direct measurements on 334 samples through a modified OFITE calcimeter measuring CO_2 pressure after 1 mn of acid attack of grounded bulk sediments with HCl 20%), and color. They were grouped into lithological classes depending on their variable proportion of detrital contents and carbonates (clayey mudstone, calcareous clayey mudstone, marlstone, argillaceous limestone/dolostone, and slightly argilaceous limestone/dolostone). The presence of bioclasts, salt/gypsum/sulfur precipitates, conglomerates, and laminated sediments was also described. These observations were complemented by XRD analysis (Goethe-Universität Frankfurt; X'Pert Pro PANalytical, Cu radiation, scans from 2° to 70° 2Θ, step size 0,1° counting time 1s) realized on 12 samples corresponding to a short core interval showing important lithological variations (512–551 m depth; Table 1).

Pollen extraction was conducted on 72 samples from the C3 core, collected between 2,9 m and 601 m depth, using HCl 30%, NaOH 10% and LST heavy liquid (d = 2) to separate the mineral from the organic fraction, HCl 30% and acetolysis (Moore et al., 1991). The identification was carried out with a photonic microscope (x500 magnification).

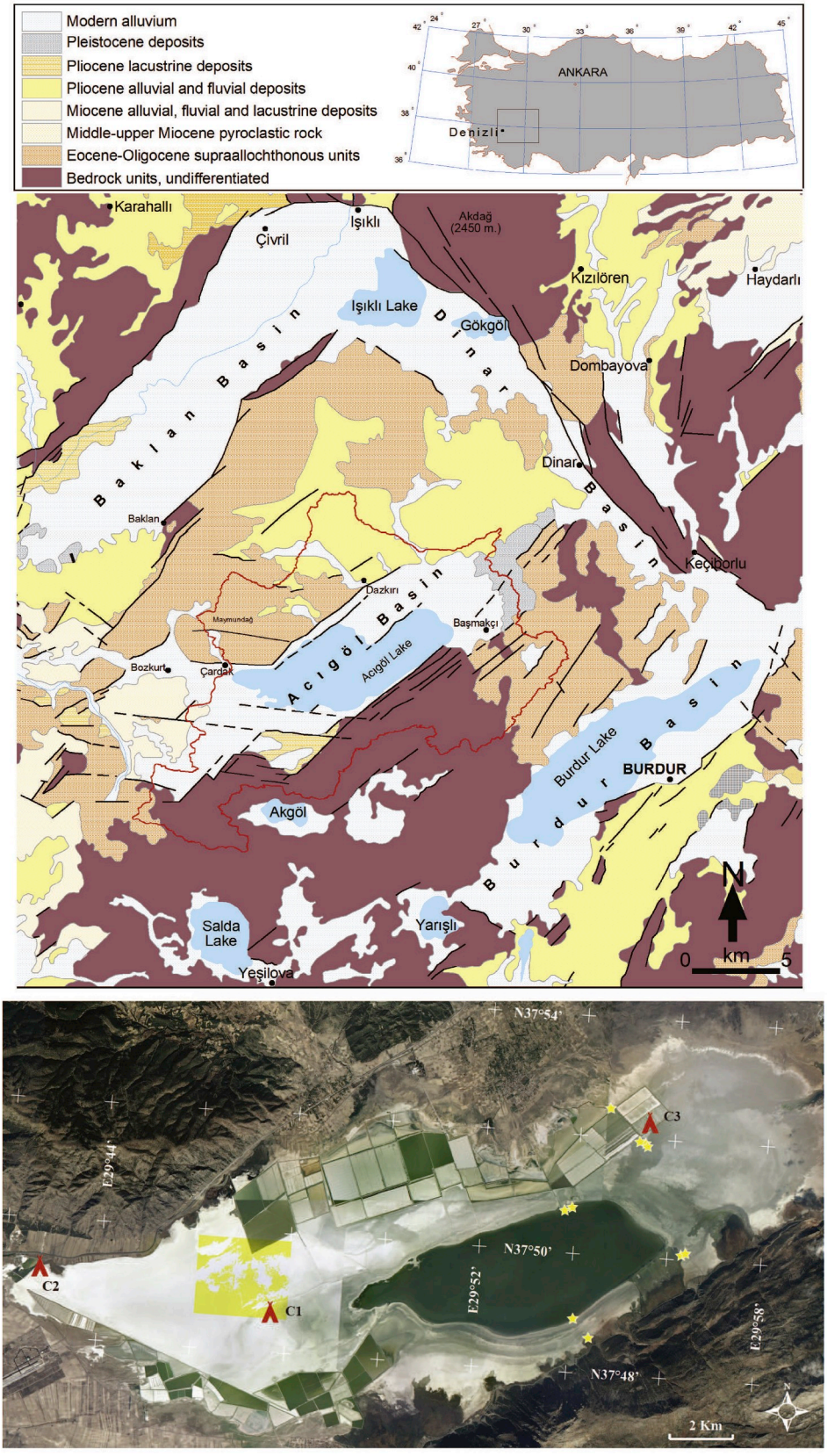

Fig. 1. Upper panel: geologic map of the Lake Acigöl area (Konak, 2002; Konak and Şenel, 2002; Şenel, 2002; Turan, 2002) and catchment area determined from Google Earth (red line). Lower panel: location of the cores (C1–C3) and modern samples (yellow stars) {ALC(1–10), ACI(1–5), ACI(7–8), D1 [C1-top]} on a satellite picture from Google Earth.

Table 1
XRF data and carbonate contents obtained by calcimetry for selected samples in the interval 512–551 m depth. Facies categories refer to: 1: clayey mudstone, 2. calcareous clayey mudstone, 3. marlstone, 4. argillaceous limestone/dolostone.

Sample	Depth (m)	Facies Category	Calcimetry %	XRD Total Carbonates	Mineralogy (XRD, relative percentages)								
					Aragonite	Calcite	Ankerite	Dolomite	Gypsum	Quartz	Feldspars	Phyll.	Others
F46	550.7	4	70.0	80.7	40.5	14.7	22.1	3.4	2.7	2.0	0.0	14.6	0.0
F54	544.2	4	70.0	85.0	40.1	10.7	31.1	3.1	2.3	1.0	1.8	9.9	0.0
F55	543.3	3	66.0	84.5	73.8	6.9	0.8	3.0	2.0	0.0	2.3	11.3	0.0
F57	541.5	2	36.0	54.2	13.3	29.9	7.5	3.4	3.3	5.1	5.4	31.9	0.0
F59	539.8	1	1.5	12.6	0.0	8.6	0.0	4.0	22.4	8.4	18.8	35.9	2.0
F63	536.5	3	52.0	67.0	29.7	20.1	12.2	5.0	3.6	2.8	4.3	22.3	0.0
F77	522.2	3	61.4	75.7	24.6	32.6	14.9	3.6	2.6	2.4	3.5	15.9	0.0
F78	521.1	4	77.0	84.1	33.4	33.8	15.3	1.6	1.8	2.3	2.7	9.0	0.0
F79	520.2	4	78.0	83.6	17.5	36.8	27.5	1.9	1.2	2.2	2.2	10.7	0.0
F82	517.9	1	16.0	33.1	5.6	19.7	2.6	5.2	8.7	7.6	16.8	33.7	0.0
F84	515.7	3	45.5	69.6	37.9	16.5	8.4	6.9	4.3	3.1	6.0	16.9	0.0
F87	512.7	3	63.9	73.2	6.6	27.2	39.4	0.0	3.2	2.0	3.9	17.8	0.0

Pollen were identified with the pollen reference collection of IMBE Laboratory (Aix-en-Provence, France), and pollen photographic books (Reille, 1992, 1995; 1998; Beug, 2004). From pollen data, we have calculated an aridity index (adapted from Fowell et al., 2003) corresponding to the ratio of *Artemisia* to Poaceae (Ar/Po). Chenopodiaceae were removed from the ratio because they are a local indicator of halophytic vegetation growing on the Acigöl lake littoral. High values of the aridity index indicate an increasing aridity of the climate and low values an increasing humidity. This index helped to interpret the magnetic susceptibility and especially the influence of the aridity state of the catchment area on the detrital input, which can be responsible for the magnetic susceptibility fluctuations. Pollen results will only be briefly reported here as they will be the main subject of a subsequent publication.

3.2. Paleomagnetism and environmental magnetism

All remanent magnetization described hereafter were measured using with the Superconducting Rock Magnetometer (SRM 560R, 2G Enterprises) of the Rock Magnetic Laboratory in CEREGE. This 3 axes magnetometer is located in a magnetically shielded room and is characterized by a noise level of ~2 10^{-11} Am^2. The studied sediments of Lake Acigöl being lithified, cores were cut in two halves and then, according to their brittle texture, core sections were either cut in 20 mm size cubic samples with a water cooled non-magnetic saw or drilled to produce small cores of 22 mm long and 25.4 mm of diameter.

In order to define the magnetic carriers of the sediments and the stability of the magnetization, 50 selected samples were subjected to Isothermal Remanent Magnetization (IRM) acquisition and measurement at 3T (supposed to be the Saturation Isothermal Remanent Magnetization SIRM) and in the opposite direction at 0.3T in order to determine the S_{ratio}, that is $SIRM/IRM_{0.3T}$. Samples were magnetized using a pulse magnetizer MMPM9 (Magnetic Measurements Ltd.). Among these 50 samples, 8 were also subjected to perpendicular IRM acquisition at 3 T, 0.3 T and 0.1 T, followed by stepwise demagnetization using the thermal demagnetizer MMTD80 (Magnetic Measurements Ltd.). Due to the weakness of the magnetic signal, only 3 samples among those presenting the strongest IRM, were subject to hysteresis and backfield measurements using a Vibrating Samples Magnetometer MicroMag 3900 (LakeShore).

188 samples, regularly distributed along the sequence, were used for paleomagnetic analysis. Demagnetization of the samples was performed either by alternating field, with the AF demagnetizer coupled to the SRM 560R, or by thermal demagnetization in a field-free oven (MMTD 80, Magnetic Measurements Ltd.). Demagnetizations were performed stepwise (up to 60–100 mT with 5 mT steps for AF treatment, up to 350–450 °C with 50 °C steps for thermal treatment). For a better removal of the secondary components of magnetization, a mixed treatment (150 °C thermal step followed by stepwise AF demagnetization) was tested without success: the thermal pretreatment implied more spurious magnetization during AF demagnetization process.

Magnetic susceptibility was measured on 566 samples with a MFK1 susceptibilimeter (AGICO, Czech Republic) in order first to trace, if present, tephra layers and second to evaluate the use of this magnetic proxy in paleoenvironmental reconstructions. For this latter aim, we compared the magnetic susceptibility with other rock magnetic parameters and pollen analyses.

3.3. Atmospheric ^{10}Be dating

Eleven samples (~1 g of dry sediment, Table S1), previously subjected to AF demagnetization for magnetostratigraphy, were selected for potential absolute dating using the atmospherically produced ^{10}Be (hereafter "atmospheric ^{10}Be dating"), following Lebatard et al. (2008). Be isotope analysis was performed at the CEREGE National Cosmogenic Nuclides Laboratory (LN2C) according to the chemical procedure set-up by Bourlès et al. (1989) and an updated separation procedure (e.g. Simon et al., 2016; Šujan et al., 2016). The authigenic ^{10}Be concentrations were determined using the spiked $^{10}Be/^{9}Be$ ratios normalized to the NIST 4325 Standard Reference Material ($2.79 \pm 0.03 \times 10^{11}$; Nishiizumi et al., 2007), measured at the French AMS national facility ASTER, and decay-corrected using the ^{10}Be half-life of 1.387 ± 0.012 Ma (Chmeleff et al., 2010; Korschinek et al., 2010). The natural authigenic ^{9}Be concentrations were measured at CEREGE using a graphite-furnace Atomic Absorption Spectrophotometer (AAS) with a double beam correction (Thermo Scientific ICE 3400®).

4. Results

4.1. Characterization of the sedimentary sequence

4.1.1. Lithology

Lake Acigöl succession shows recurrent variations between more carbonate-rich (limestone/dolostone) and more detrital-rich (clayey mudstone) sediments. Five main facies were created according to these variations in carbonate content, as determined by visual observation and calcimeter measurements (Fig. 2). With regards to long-term lake dynamics, siliciclastic-rich intervals are more frequent towards the upper half of the sequence, while high-carbonate types dominate the lower part, with a maximum around 500-450 m depth. Superimposed on this trend, shorter-term variations in the lake succession are visible through the regular alternation of intervals richer in carbonates or detrital siliciclastic fractions. The macroscopic biological components of Lake Acigöl comprise undifferentiated shell fragments, ostracods, gastropods, and bivalves. Shell fragments are widely present throughout the core, except in the upper ca. 70 m, although some intervals are more enriched

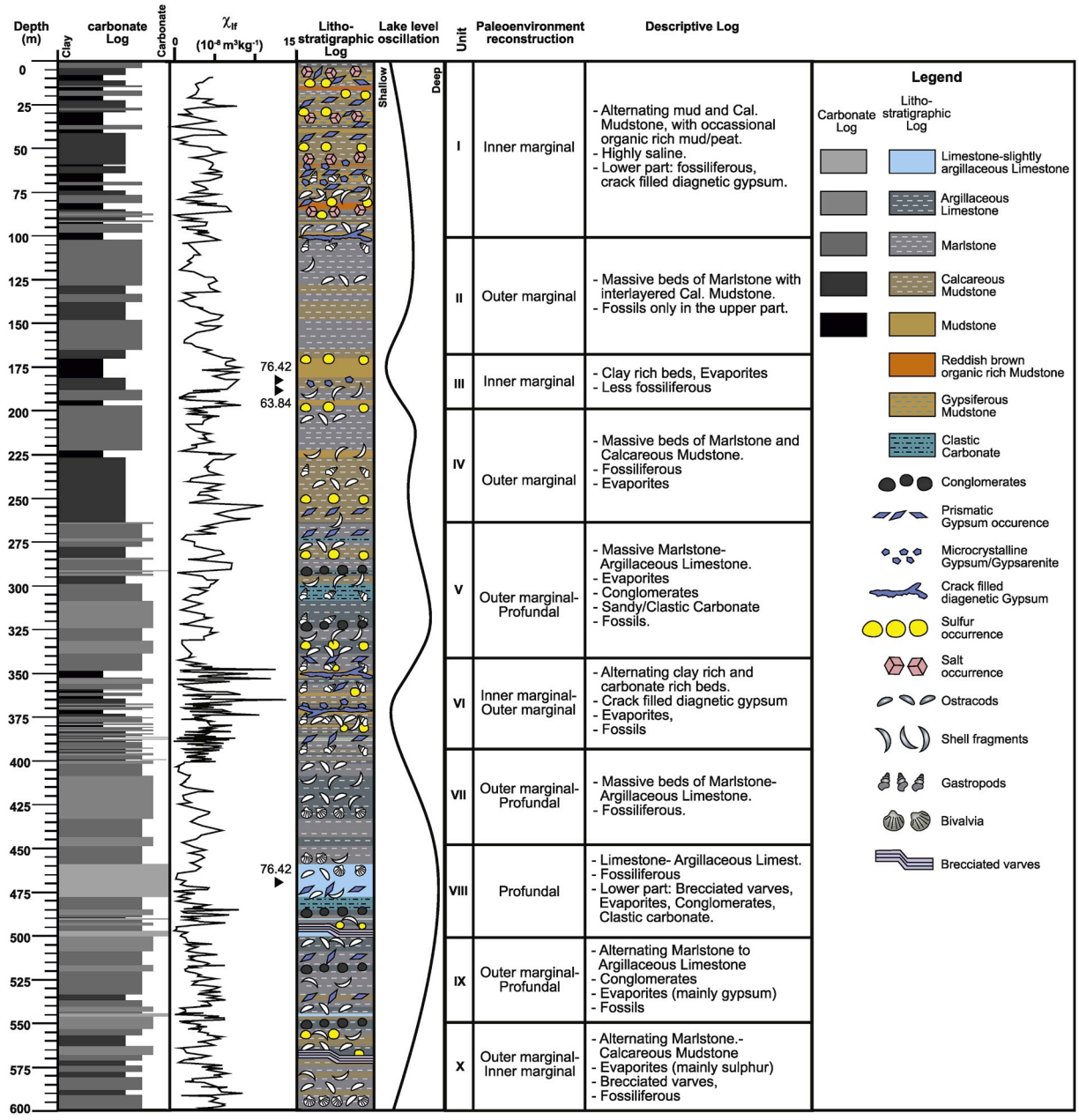

Fig. 2. Description of the sedimentary succession with from left to right: carbonates vs. clays profile, magnetic susceptibility, lithostratigraphic log and interpretation in terms of water level and deposit environment. N.B. "Limestone" here includes both calcitic and dolomitic limestone as well as dolostone.

than others (Fig. 2). Ostracods, relatively frequent in the lower 2/3 of the sequence, become rarer above 250-200 m depth, and similarly to shell fragments, are absent from the uppermost sediments. Gastropods seem restricted to the interval ca. 400-70 m depth, with a maximum at 400-275 m depth. Bivalves are only sporadically observed in the lower part of the core, up to ca. 450-400 m depth. Finely laminated layers, differentiated by color (beige to grey), can be observed at different depths along the core (Fig. 2). They may correspond to shifts in the sediment type (carbonate/siliciclastic components) related to rapidly fluctuating environmental conditions. Such laminations are usually preserved in freshwater when bioturbation is limited by anoxia and sufficient depth protects the sediments from currents and erosion, and/or when sedimentation rates are high (e.g. Glenn and Kelts, 1991). These conditions are frequently encountered in meromictic lakes, where layers of water with different densities present at different depths do not mix (e.g., Anderson et al., 1985; Zolitschka et al., 2015). Mineralogical composition of sediments of the 512–551 m depth interval through XRD measurements show various proportions of aragonite, calcite, ankerite (Ca(Fe,Mg,Mn)(CO3)2), dolomite, gypsum, quartz, feldsdpars and phyllosilicates (Table 1). In the carbonate phases, the respective amount of aragonite and calcite vary greatly, seemingly independently from carbonate contents, and may be related to complex interplay between precipitation and preservation patterns (e.g., Roeser et al., 2016). The amount of dolomite is generally low (below 7%) in this interval. The siliciclastic detrital phase is dominated by phyllosilicates. A comparison between carbonate contents as measured by calcimeter analysis and XRD (Table 1) shows that the former capture correctly the carbonate content variations, but usually underestimate their amount, suggesting that only part of the ankerite/dolomite phases are measured though calcimeter analyses. Gypsum is a frequent feature of the Lake Acigöl sediments. It occurs under the form of massive and prismatic gypsum (Helvaci et al., 2013), which can be considered as primary and

precipitated due to high evaporation rates. On the other hand, the gypsum filling cracks can be considered diagenetic, and originating from sulfate-rich water circulation through the fractures. Furthermore, the occurrence of nodular sulfur throughout the core can be attributed to the transformation of gypsum into sulfur by the reducing action of microbial activity (Mutlu et al., 1999; Helvaci et al., 2013). From the XRD results on the interval 512–551 m depth (Table 1), gypsum usually stays below 5%, but markedly increases in the two intervals with the lowest carbonate contents.

All lithological observations confirm a general trend towards shallower lacustrine environments through time, as already assessed by Helvaci et al. (2013), and possibly with a transition from fresh-brackish (lower part) to brackish-saline (upper part) that would have limited biota diversity and reduced, notably, the number of ostracod species able to cope with increased salinity (see Altınsaçlı and Mezquita, 2008). Furthermore, finely laminated layers are almost exclusively restricted to depths below ca. 200 m (Fig. 2). This suggests that above this depth, lake levels were too shallow to allow preservation of fine laminations. Additionally, the increased proportion of gypsum and sulfur at ca. 350–400 m and 175–200 m depth, as well as in the upper 100 m of the core (Fig. 2), suggest high evaporation rates and evaporative precipitation during these periods. Halite is also observed in the upper 100 m sediments, which implies that Lake Acigöl then entered in its most saline condition; peat/soil facies are even recorded sporadically in the uppermost sediments, inferring partial emersion.

The simultaneous increase in detrital input and evaporate precipitation suggests low lake stands. Reversely, carbonate deposits would correspond to high lake levels and are probably induced by enhanced carbonate endogenic production favoring higher biodiversity. The lithological succession at Lake Acigöl can therefore be translated into phases of lake expansion and contraction, with successive facies reflecting inner marginal (detrital-rich) to profundal (carbonate-rich) environments (Fig. 2). Regressive phases are thus represented by a change from carbonate-rich to silicoclastic-rich facies.

Periodic disturbance of the sedimentary depositional system can also be observed. Brecciated laminated layers (490 and 570 m depth), as well as irregular cracks filled by diagenetic gypsum (367 and 377 m depth), suggest tectonic activity creating local fractures into already indurated or semi-indurated sediment. Conglomeratic levels (occasionally observed in the 480–550 and 290–320 m depth intervals) suggest the remobilization and transport of sediments towards deeper lacustrine environments, which could be brought up by either seismic activity or gravity instability of the lake slopes, or a strong local discharge of terrestrial deposits via, e.g. stream activity.

According to this model and observations, Lake Acigöl first underwent a relative deepening (ca. 600-450 m depth), possibly created by tectonic activity, followed by a general shallowing-up to the present-day (Fig. 2), interrupted at ca. 350 m depth by another less marked, potentially tectonically-induced relative increase in lake levels. Shorter-term, pseudo-cyclic fluctuations between siliciclastic and carbonate-rich intervals (Fig. 2), however, suggest a superimposed factor controlling sedimentation patterns in Lake Acigöl, and notably the variations between carbonate production, evaporative processes, and detrital input; this is likely to correlate with major recurrent climatic fluctuations during the Quaternary, in particular linked to glacial/interglacial cycles.

4.1.2. Magnetic susceptibility

Magnetic susceptibility (MS) ranges from $-0.18*10^{-8}$ to $14*10^{-8}$ m^3kg^{-1} (Fig. 2), with two spikes above $60*10^{-8}$ m^3kg^{-1} marking the occurrence of two tephra layers at ~ 190 m and at ~ 470 m respectively. The volcanic tephra found at 470 m depth was tested for radiometric Ar/Ar dating. Unfortunately, due to the small size of the volcanic particles (≪200 μm) and their alteration, this attempt was unsuccessful. The susceptibility record used hereafter was cleaned from data marking tephra layers.

Comparing magnetic susceptibility to sedimentary features, there is an overall correlation between MS and facies (Fig. 3A). Indeed, the average magnetic susceptibility for a given facies decreases when the carbonates (diamagnetic material) increase.

The comparison between magnetic susceptibility and carbonate content (Fig. 3B) show a weak anticorrelation due to the dispersion of magnetic susceptibility data, especially for samples with low values of carbonates content. This observation shows the rather limited effect of the paramagnetic and ferromagnetic dilution by diamagnetic carbonate content. Comparing the magnetic susceptibility with Saturation isothermal magnetization (Fig. 3C), there is also a weak correlation whatever the ferromagnetic mineralogy (scattered S ratio in Fig. 3C). Therefore, the magnetic susceptibility is not only modulated by the ferromagnetic input but also by the paramagnetic component (clays). Consequently, the magnetic susceptibility variation is rather due to fluctuations in detrital input assemblage with variations of the relative contribution of paramagnetic and ferromagnetic particles. These fluctuations are probably due to changes in the catchment area.

Preliminary pollen analyses show that the vegetal landscape remains mostly open and arid throughout the sedimentary record. The average rate of arborean pollen is 28% of the Pollen Sum (PS) with a minimum of 3.5% of the PS at 597 m depth (2.3 Ma) and a maximum of 91% of the PS at 155 m depth (0.58 Ma). In order to estimate if there is any relationship between the state of the catchment and the magnetic susceptibility data, we compared the latter to an aridity index (Ar/Po) estimated from pollen analyses. For significantly high values of the aridity index (higher than 5), there is a good agreement between an increase of both aridity and steppic vegetation, and an increase in magnetic susceptibility (Fig. 3D). This corroborates the interpretation that increases in magnetic susceptibility are linked to more detrital input due to less vegetal cover in the surrounding area inducing more erosion. The high variability of susceptibility for sediments characterized by low carbonate content may be linked to varying sedimentary sources (proximal vs. distal) in the catchment area.

4.2. Age model

4.2.1. Magnetostratigraphy

4.2.1.1. Rock magnetism and magnetic carriers. S_{ratio}, which reveals the relative abundance of high and low coercive magnetic minerals (e.g. Stober and Thompson, 1977; Bloemendal et al., 1992; Liu et al., 2007), varies from 0.8 to 0.99 mainly indicating that a low coercivity mineral dominates the IRM signal. Even though there is no clear relationship between S_{ratio}, SIRM and NRM, SIRM values are between 100 and 500 times higher than NRM values (Fig. 4A), a range coherent with a NRM signal free from accidental acquisition of secondary magnetization due to lightning or to the vicinity of permanent magnets.

Thermal demagnetization of IRM informs on magnetic mineral types according to their coercivity (Lowrie, 1990; Fig. 4B). Indeed, the low coercive fraction (up to 0.1T) show progressive and rather constant unblocking up to the Curie temperature of magnetite (580 °C) at which IRM reached zero. Nevertheless, there are some inflexions in the unblocking patterns at ~300 °C. In addition, the medium coercivity fraction (up to 0.3T) shows a decay at ~300 °C. These features illustrate the occurrence in some samples of a medium coercivity mineral losing its magnetic signal at ~300 °C (in agreement with an S-ratio below 0.95). It could be therefore an iron sulfide such as Pyrrhotite. The high coercivity fraction, in spite of noisy pattern linked to oxidation processes during heating, does not show significant contribution of hematite.

Characteristic parameters deduced from hysteresis loops and backfield curves show H_{cr}/H_c and M_{rs}/M_s lying in the area of the pseudo-single domains (Day et al., 1977, Fig. S1). According to the thermomagnetic results, the sediments most likely mainly contain fine grains of magnetite, probably of detrital origin, even though mixture of different grain sizes cannot be ruled out (Dunlop, 2002).

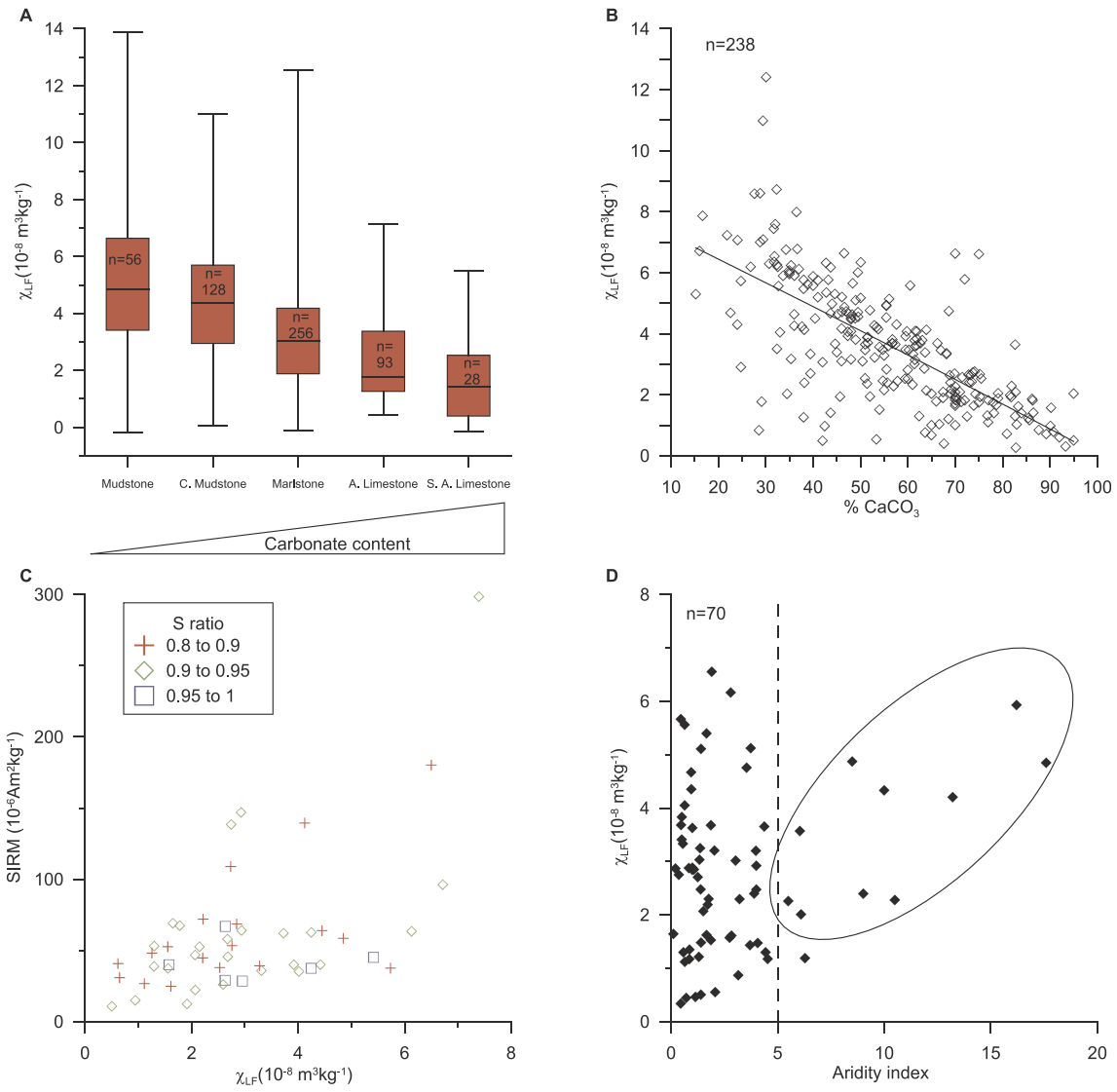

Fig. 3. Comparison of magnetic susceptibility (MS) with other proxies: A. MS vs. facies: the box-whisker box shows that the general autocorrelation with facies is confirmed. N.B. "Limestone" here includes both calcitic and dolomitic limestone as well as dolostone. B. MS (corrected from carbonates contribution) vs. carbonates content. The Linear regression displays only a rough relationship since magnetic susceptibility is not only affected by (diamagnetic) carbonate dilution. C. MS vs SIRM and Sratio: there is a poor correlation between MS and SIRM and S ratio values are scattered. D. MS vs. an aridity index deduced from pollen analysis: there is a positive relationship for aridity index >5, i.e. when the aridity index is significant.

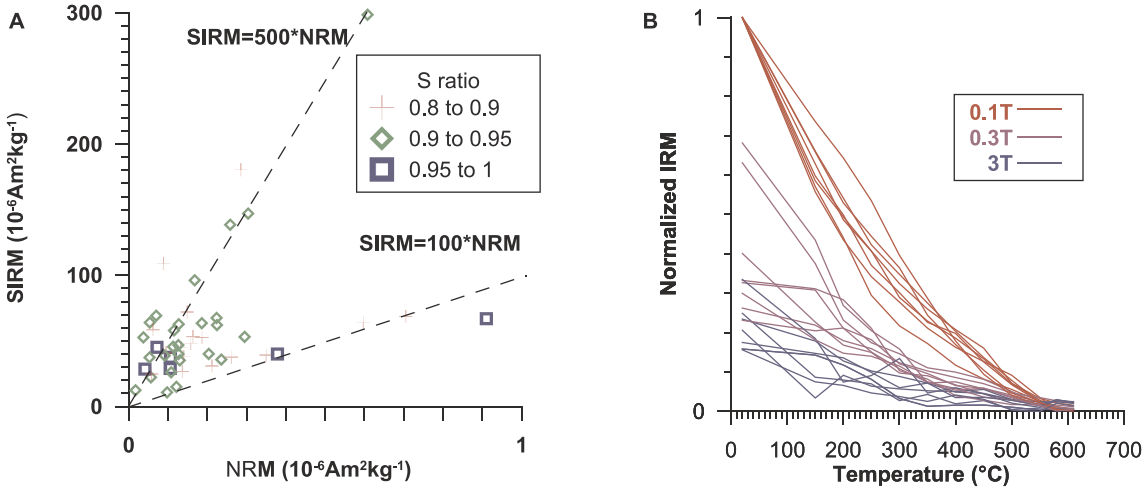

Fig. 4. A. NRM intensity changes as a function of SIRM; B. Thermal demagnetization of orthogonally acquired IRMs at 3T, 0.3T and 0.1T

The rock magnetic study shows therefore that magnetite, likely detrital, is the predominant carrier of magnetic signal making possible a paleomagnetic dating approach.

4.2.1.2. Magnetic chrons determination. As expected for low intensity of NRM ranging from 2.8 10^{-8} to 8.6 10^{-7} Am^2kg^{-1} (except for tephra in which NRM of 3 10-5 Am^2kg^{-1} is reached), the demagnetization diagrams are often noisy but characteristic remanent magnetizations (ChRMs) could be retrieved from two thirds of the samples. Only 18 samples present a single component of magnetization that allows a very good least square analysis (large NRM fraction and maximum angular deviation -MAD- lower than 5°, Fig. 5A and B). These high-quality results could be found in normal as well as in reversed polarity sections and will be considered as key points for the rest of the analysis (category A, black dots in Fig. 6A). For the others (category B, white dots in Fig. 6A), either the least square analysis was possible only on a small fraction of the demagnetization path (Fig. 5C), or the ChRM was estimated through great circle analysis (Fig. 5D), or only a stable end-point could be defined (Fig. 5E). In these cases, the ChRM can still be influenced by secondary components of magnetization not properly removed, i.e. intermediate component of magnetization.

Since the vertical axis is the only reference, only inclination data can be retrieved from the magnetostratigraphic column (Fig. 6A). The current expected inclination in the studied area is 55° (IGRF-12, https://www.ngdc.noaa.gov/IAGA/vmod/igrf.html), similar to the 54° expected 5 Ma ago (Besse and Courtillot, 2002). Conservatively, an uncertainty of 25° around the expected value was assumed to differentiate between stable and transitional directions. This large uncertainty range is supposed to account for the common inclination flattening in sedimentary rocks, as well as for un-removed secondary components of magnetization, or orientation errors. This analysis evidences 49 normal, 40 reverse, and 36 transitional directions, which defines several geomagnetic polarity changes (Fig. 6A).

Relying on the key points and an optimization of the sedimentary rates (Fig. 6B), the Brunhes/Matuyama transition (781 ka) is confidently located at around 210 m while the Jaramillo (988–1172 ka) and Olduvai (1778–1945 ka) normal subchrons (Ogg et al., 2012 and references therein) can be identified between 270-290 m and 450–495 m, respectively. Other samples may have recorded some reverse subchrons in the Brunhes normal chron, as well as the Cobb Mountain and Reunion normal subchron in the Matuyama reverse chron, but we did not try to interpret these short events, hard to differentiate with possible inversion of the vertical axis due to accidental upside down flip of core fragments.

Downward extrapolation of the derived age model (Fig. 6B) leads to a core bottom age around 2.3 Ma.

The deduced sedimentation rates (23–29 cm/ka) agree perfectly with a chemical cyclostratigraphy (from ITRAX measurements on U-channel) performed on the upper 170 m of soft sediments by an

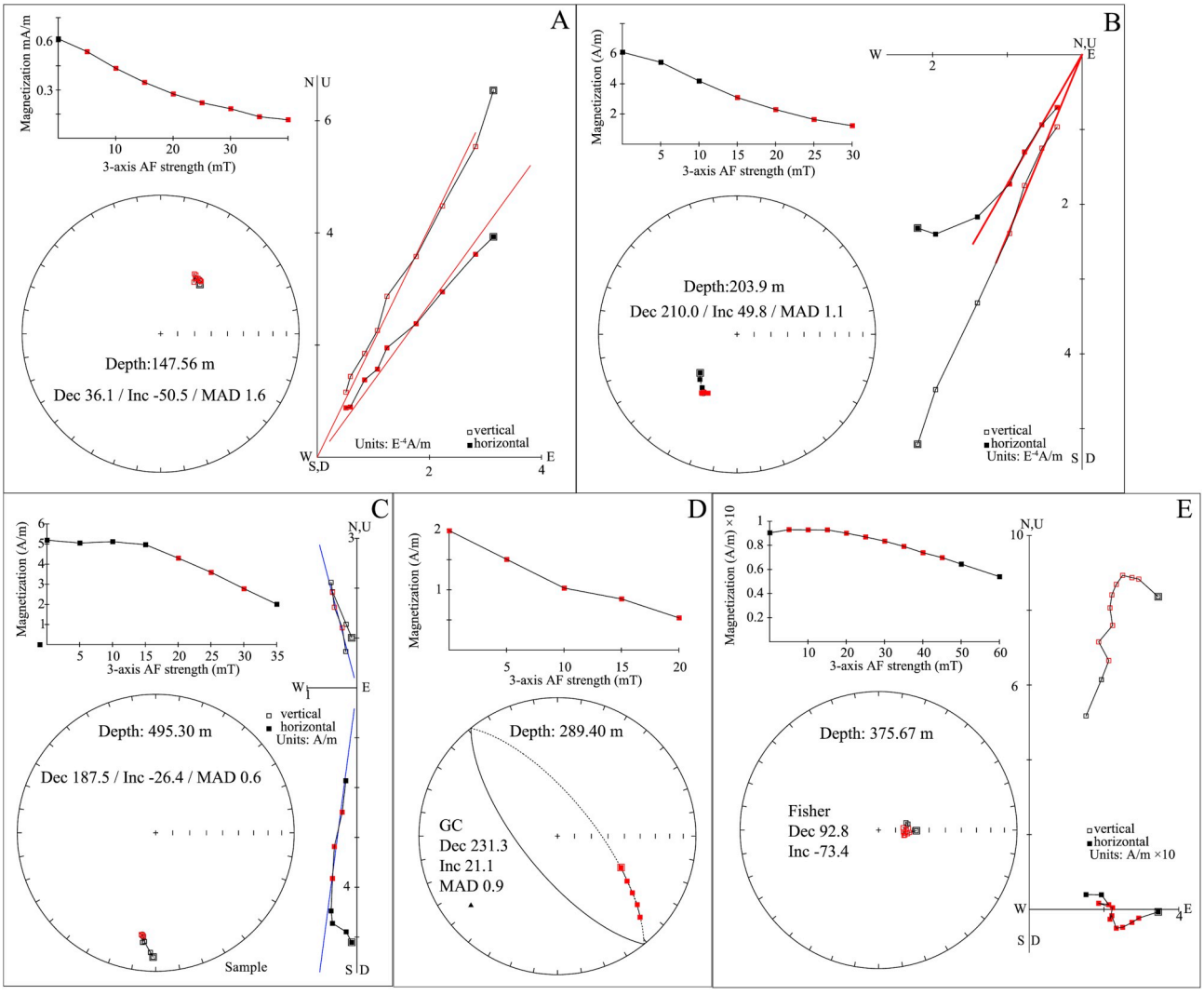

Fig. 5. Demagnetization analyses. Full/open squares are upper/lower hemisphere for the equal-area plots and horizontal/vertical component on the ortogonal plots. Points used for a calculation are in red. PCA/GC/F correspond to Principal Component Analysis/Great Circle/Fisher estimations, respectively.

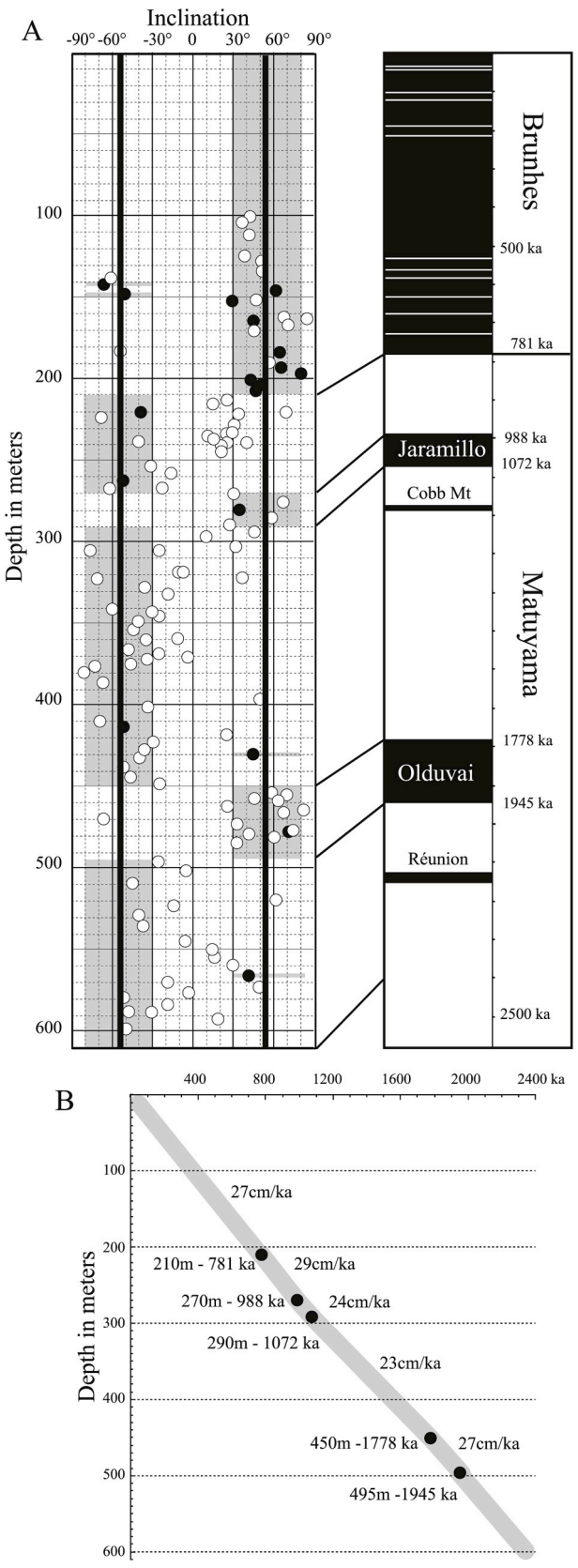

Fig. 6. A. Variation of the inclination as a function of depth and correlation with the global polarity timescale (Ogg et al., 2012). B. variation of the sedimentation rate as a function of depth.

independent team (Akçer-On et al., 2016), who estimated an age around 700 ka BP at 170 m (24 cm/ka).

4.2.2. *Atmospheric ^{10}Be measurements*

The atmospheric ^{10}Be ages were calculated using the classical radioactive decay equation $N_{(t)} = N_0 * e^{-\lambda t}$, where $N_{(t)}$ is the authigenic ^{10}Be/^{9}Be ratio measured in the sample to date, N_0 is the initial authigenic ^{10}Be/^{9}Be ratio, λ is the ^{10}Be radioactive decay constant and t is the time elapsed since deposition. To obtain a reliable age, two requirements are needed: 1) the initial authigenic ratio N_0 has to be accurately determined; and 2) after deposition, the system should have remained closed (i.e. isolated from inputs/outputs of both beryllium isotopes).

To determine the initial authigenic ratio N_0 characteristic of the Acigöl Basin (Lebatard et al., 2008, 2010; Novello et al., 2015; Šujan et al., 2016), modern samples were collected (Fig. 1, Table S1). The ALC (1–10) semi-dried clay-samples were collected in 2015 in the vicinity of the C3 coring location but within the decantation basins of the ALKIM operating area. They were therefore composed of a large proportion of gypsum that had to be removed manually as much as possible before analysis. Considering the dispersion of the thus obtained N_0 values, new samples were collected in 2016 away from industries: i) the ACI(1–5) samples along the south margin of the lake, in two areas seasonally covered by water (within the lake and at its dried edge); ii) the ACI(7–8) samples drowned under ~25 cm of water, on the north side of the perennial flooded lake. Finally, the D1 sample, a proxy for the not useable C3 top, has been taken at the top of the C1 core.

The authigenic ^{10}Be/^{9}Be ratios (ranging from 0.42 to 2.42×10^{-8}, Table S1) measured for the modern sediment samples are similar to the authigenic ^{10}Be/^{9}Be ratio measured on recent surficial continental sediments (e.g. Graham et al., 2001; Šujan et al., 2016). However, they are scattered despite the small size of the area investigated, with a 47% dispersion in the Kernel Density Estimation (KDE, Fig. 7A; Vermeesch, 2012), and four peak values modelled at $0.44*10^{-8}$, $0.79*10^{-8}$, $1.04*10^{-8}$ and $2.25*10^{-8}$.

In the absence of a statistically significant value of the initial (modern) authigenic ^{10}Be/^{9}Be ratio of the modern samples, the radioactive decay equation was used to compute an initial ratio from each ^{10}Be/^{9}Be ratio measured for all core samples, their ages being derived from the magnetostratigraphic age model. The density plots present an even larger range of values whose overall dispersion is 57%. Only two of the resulting five N_0 peak values ($1.03*10^{-8}$, $1.61*10^{-8}$, $2.23*10^{-8}$, $3.93*10^{-8}$, and $9.59*10^{-8}$, Fig. 7B) are similar to those evidenced using the modern samples approach: the $1.04*10^{-8}$ 2.25×10^{-8} peaks (Fig. 7A). The surface samples, whose N_0 values are close to 2.25×10^{-8}, are those that have been collected under ~25 cm of water at the north lake margin, within the perennial lake. As these samples are likely more reliable to determine the N_0 value, this value was favored and used to calculate atmospheric ^{10}Be ages. About five of the thus-defined authigenic ages agree with the magnetostratigraphic values (Fig. 7C).

Considering i) that the watershed supplying the lake is affected by tectonics, which very likely implies temporally variable inputs of ^{9}Be; ii) that the reduced size of the lake does not favor the homogenization of the solubilized fractions of the beryllium isotopes which have different sources; and iii) the high gypsum concentration of the analyzed sediments, the use of the atmospheric ^{10}Be dating method in Lake Acigöl does not take place under the most favorable conditions. Still, results are not unrealistic, with an atmospheric ^{10}Be age range on average coherent with the magnetostratigraphic age model.

5. Dated magnetic susceptibility and sedimentary facies records: clues for a potential paleoclimatic archive

The dated and smoothed (5 points running average, i.e. a circa 5 ka window) magnetic susceptibility data show fluctuations in the 10–100 ka time window (Fig. 8) interpreted as reflecting changes in clay detrital

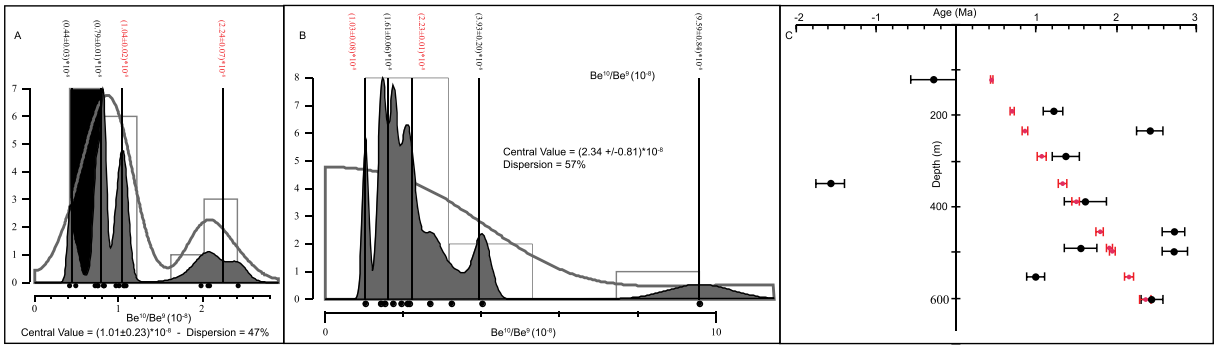

Fig. 7. Density plot of N_0 ratios calculated for the modern samples A. using the authigenic $^{10}Be/^{9}Be$ ratios measured for the modern sediment samples and B. using the radioactive decay equation and the magnetostratigraphy based age model. The central values are overall weighted mean values; the peak values correspond to weighted means of sub-populations within the total distribution. C. Modelled core sample ages using 2.25×10^{-8} (black dots) as the authigenic initial $^{10}Be/^{9}Be$ ratio (N_0) compared to the ages derived from the age model based on magnetostratigraphy (red dots).

input, which agree with main variations in the sedimentary facies (i.e., more or less carbonated deposits). These short-term pseudo-cycles are accompanied by a longer-term trend visible in the sedimentary facies evolution, towards less carbonated deposits upward. When compared to a climatic record of global significance like Benthic $\Delta^{18}O$ from deep sea cores from North Atlantic (Lisiecki and Raymo, 2005, Fig. 8) a correlation can be drawn between high detrital (siliciclastic) input into Lake Acigöl, low carbonate contents, and high benthic $\Delta^{18}O$, which is interpreted as marking glacial periods throughout the Quaternary. According to the rather limited number of magnetic susceptibility data (569) and the time window of 2.3 Ma, no spectral analysis could be performed. The long-term evolution of Lake Acigöl towards less carbonated facies, interpreted as a progressive shallowing-up of the lake system throughout the Quaternary, also mirror the general trend from the north Atlantic foraminifera isotopic record towards cooler conditions. These observations suggest a strong control of climatic patterns over the sediment record at Lake Acigöl. The high frequency variations are their relation to global climatic fluctuations are especially clear for the last 700 ka. For this time interval, we could easily identify the last 16 Marine Isotopes Stages, especially the glacial periods marked by increases in magnetic susceptibility and clay proportion in Lake Acigöl sediments. An attempt to match one by one the climatic transitions between the Lake Acigöl sedimentary record and the marine $\Delta^{18}O$ record suggests significant time lags. Despite possible delay in continental responses to global climatic changes (Demory et al., 2005), we rather attribute these lags to imprecisions in the age model that is built using 5 points of paleomagnetic correlations for the last 2.3 Ma. Therefore, due to the resolution of the study, high frequency changes in sedimentation rates cannot be detected that may affect the correlation between Lake Acigöl and global paleoclimatic records.

In Lake Acigöl, high detrital input, reduced carbonate precipitation, and enhanced evaporative contents mark low lake levels, and point to generally drier conditions. The comparison of sedimentary, magnetic, and oxygen isotope records from the North Atlantic suggests the association of such drier intervals with global glacial periods. Following this we can propose that during interglacial periods carbonate deposition in

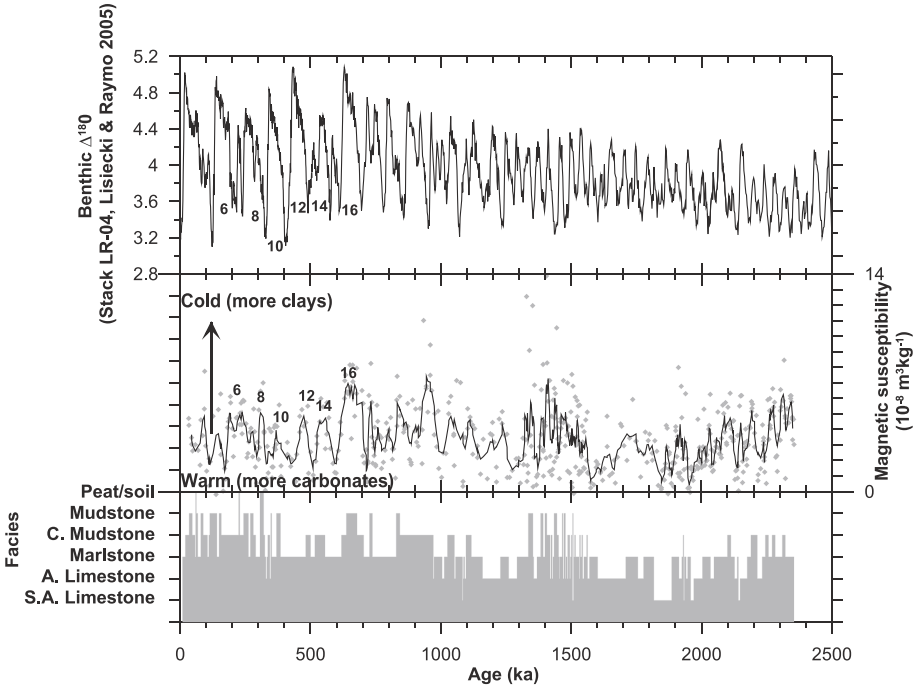

Fig. 8. Dated facies and magnetic susceptibility records (with a running average every 5 data) compared with the $\Delta^{18}O$ stack of Lisiecki & Raymo (2005). Numbers indicate glacial marine isotope stages and their corresponding deposits in the Acigöl sedimentary sequence. N.B. "Limestone" here includes both calcitic and dolomitic limestone as well as dolostone.

Lake Acigöl was favored by higher lake levels, reduced detrital input, and high insolation favoring productivity and hence carbonate precipitation. High vegetation cover in the catchment area was probably reducing detrital input to the lake, resulting into a magnetic susceptibility decrease in the sediment record. During glacial periods dry conditions in SW Anatolia were leading to increased evaporite deposition, detrital input through the denudation of the catchment (potentially both through sheet floods and aeolian input), and reduced carbonate deposition. This model is strengthened by the results of the aridity index calculated from pollen analyses that show a good correlation between increases in magnetic susceptibility and therefore the clay content, and increases in aridity (Fig. 3D).

Although no record in the Mediterranean region covers more than a fraction of the Quaternary period, a combination of high water levels, high carbonate productivity, low detrital input, and increased vegetation cover in the catchment corresponding to interglacial cycles were proposed for several lake successions. The record of Lake Van in Eastern Anatolia, covering the last ca. 600 ka, shows that low lake levels were correlated with glacial periods and associated to global climatic cycles through low precipitation (Cukur et al., 2014). For the last 360 ka, i.e. the last four glacial-interglacial cycles (Kwiecien et al., 2014), an association was established through pollen, lithological observations and geochemical analyses, between cold and dry glacials, versus warm and wet interglacials, with full interglacials conditions being marked by either high or slowly falling water levels. In Lake Yammoûneh (Lebanon; northern Levant), the sedimentary succession, which covers the last ca. two glacial-interglacial alternations (last ca. 250 ka), authigenic and biogenic calcite get preferentially deposited in interglacial periods under warm and wet conditions, in association with higher arboreal cover and low catchment erosion (Develle et al., 2011; Gasse et al., 2011). The Lake Yammoûneh record also shows a general trend towards less effective moisture availability, which was put in correspondence with the general weakening of solar insolation associated with decreasing amplitude in the eccentricity cycle (Gasse et al., 2011). In Lake Ohrid (Macedonia/Albania), for the last 647 ka, interglacials are marked by high primarily production in summer and enhanced calcite precipitation (Francke et al., 2016). By contrasts, lake sediments from the Southern Levant (Dead Sea basin) record higher lake stands during glacial periods (Develle et al., 2011), which may denote a different major climate-related control on water levels, i.e. reduced evaporation during the colder and drier conditions of the glacial periods.

Fluctuations of lake levels and the alternation of palustrine (even alluvial), detrital-rich deposits with lacustrine, carbonate-rich sediments were additionally well-recorded in long-term Miocene deposits and associated to orbital cycles regulating insolation input. Amongst others, records form NE Spain (Calatayud Basin – Orera section; Abdul Aziz et al., 2000, 2003, Van Vugt et al., 2001; Teruel Basin - Prado section; Abels et al., 2009a, b), show alternations between marl/clay layers reflecting lake margin mudflats and lacustrine carbonates, and are interpreted as reflecting orbital cycles. Cyclicities at Orera were recognised at the precession time-scale (19 ± 23 kyr) and, less clearly, at the larger-scale eccentricity cycles (400 and 100 ka; Abdul Aziz et al., 2000; Van Vugt et al., 2001). Transitions from lake lowstands to highstands are attributed to changes from dry to wet conditions, related, respectively, to insolation minima and maxima.

All the records from the northern and north-eastern Mediterranean, both from the Quaternary and the Miocene, propose an association of colder and drier conditions, leading to decreasing lake levels and lower carbonate productivity during the glacial intervals. In this respect, the Lake Acigol records is perfectly in accordance with the pattern established from other local records from the Northern and Eastern Mediterranean, at the exception of the Southern Levant.

The long-term evolution of Lake Acigöl towards shallower depositional patterns probably results from the interplay between a general shift in climate conditions and sedimentation infill processes. Since the lake has no outlet and no major influx, and therefore acts as a closed system, constant sediment infill, if not balanced by subsidence, would result into lake level shallowing with time. On the other hand, a general trend towards a more negative precipitation-evaporation balance (e.g., through the establishment of a drier climate) would strengthen this evolution (such as suggested in the record from Lake Yammoûneh for the last two glacial-interglacial cycles; Gasse et al., 2011). However, despite the relative stability of sedimentation rates throughout the sedimentary column arguing in favor of a stable sedimentary system, the sedimentary succession at Lake Acigöl shows a maximum water level dated at around 1.8 Ma, which excludes a simple correlation between climatic trends and sedimentation type on a long-term perspective. Long-term water level changes in Lake Acigöl can therefore be associated to a combination of a long term global cooling for the last 2.3 Ma, and subsidence changes due to the tectonic activity that would induce an increase in water depth.

Reconstructing paleoclimatic signals from the sediments of Lake Acigöl would imply to properly delineate the respective role of climate and tectonics on lake levels (tectonic forcing factors were also reported to probably affect lake levels and sedimentation patterns at Lake Van; Cukur et al., 2014); being able to differentiate between detrital and authigenic carbonate/gypsum depositions; and assessing the origin of detrital elements to the lake (flood sheets versus aeolian input). For example, in Lake Yammoûneh (Develle et al., 2011), detrital input is mostly attributed to an aeolian provenance, due to the dominantly carbonated nature of the surrounding bedrock. At Lake Acigöl, preliminary observations suggest a more proximal source for detrital inputs, coming from either the erosion of the local bedrock or of former alluvial/lacustrine deposits.

6. Conclusion

Lake Acigöl is the longest chronological constrained lacustrine record in western Asia, covering the entire Quaternary Period, with a bottom age of 2.3 Ma and rather stable sedimentation rates ranging from 23 to 29 cm ka^{-1} based on magnetostratigraphy.

Conditions are not the most favorable to apply the atmospheric ^{10}Be dating technique, but results from this method are not totally unrealistic, with authigenic ^{10}Be ages that support the magnetostratigraphic age model.

Long term evolution of the lake from (carbonate-rich) deep facies to inner marginal (detrital and evaporites-rich) facies is probably related to both the local tectonic activity and the long term climatic change over the whole Quaternary.

High frequency changes are depicted in magnetic susceptibility record supported by pollen and sediment analyses (facies, carbonate content and XRD) for the last two million years. Despite some time lags due to the resolution of the chronological constrains, glacial/interglacial patterns seem to be clearly recorded in Lake Acigöl sediments with warm periods characterized by high carbonate (diamagnetic) production and cold and dry periods characterized by high detrital (paramagnetic and ferromagnetic) input.

Acknowledgments

This research was funded by TUBITAK-CNRS bilateral cooperation with the grant number of 114Y723 during 2015–2017. The funds by 1) the ECCOREV Research Federation (OSU PYTHEAS, CNRS, AMU) for the project “ACIGOL”, 2) the Labex OT-MED (OSU PYTHEAS, CNRS, AMU) for the project BILAT, 3) and the projet EPICA (INSU 2018; Programme Tellus-INTERVIE) were received during 2017–2018. We thank the Wissenschaftliche Gesellschaft Freiburg im Breisgau for additional funding. We acknowledge the ALKIM Company for permitting us access and sampling to the core with special gratitude to Mr Hüseyin Ünlü (MSc) who was the director of ALKIM Company in Acigöl during the sampling and Mr. Mahmut Eser (MSc), the manager of the exploitation and Mr. Ünal Arık, present director of the company. The ASTER AMS

national facility (CEREGE, Aix en Provence) is supported by the program INSU/CNRS INTERVIE, the ANR through the "Projets thématiques d'excellence" program for the "Equipements d'excellence" ASTER-CEREGE action and IRD. We thank S. Choy and L. Gacem for their help in the ^{9}Be measurements using the AAS of the LN2C (CEREGE). The data are archived at https://dx.doi.org/10.1594/PANGAEA.907658.

Appendix A. Supplementary data

Supplementary data to this article can be found online at https://doi.org/10.1016/j.quageo.2019.101038.

References

Abdul Aziz, H., Hilgen, F.J., Krijgsman, W., Sanz-Rubio, E., Calvo, J.P., 2000. Astronomical forcing of sedimentary cycles in the middle to late Miocene continental Calatayud Basin (NE Spain). Earth Planet. Sci. Lett. 177, 9–22. https://doi.org/10.1016/S0012-821X(00)00035-2.

Abdul Aziz, H., Krijgsman, W., Hilgen, F.J., Wilson, D.S., Calvo, J.P., 2003. An astronomical polarity timescale for the late middle Miocene based on cyclic continental sequences. J. Geophys. Res. 108 (B3), 2159. https://doi.org/10.1029/2002JB001818.

Abels, H.A., Abdul Aziz, H., Ventra, D., Hilgen, F.J., 2009. Orbital climate forcing in mudflat to marginal lacustrine deposits in the Miocene Teruel Basin (North-East Spain). J. Sediment. Res. 79, 831–847. https://doi.org/10.2110/jsr.2009.081.

Abels, H.A., Abdul Aziz, H., Calvo, J.P., Tuenter, E., 2009. Shallow lacustrine carbonate microfacies document orbitally paced lake-level history in the Miocene Teruel basin (North-East Spain). Sedimentology 56, 399–419. https://doi.org/10.1111/j.1365-3091.2008.00976.x.

Akçer-Ön, S., Bora Ön, Z., Çağatay, N., Helvaci, C., Acar, D., Bauchi Danladi, I., 2016. Caba 2016. High Resolution Climatic Records of Western Anatolia for the Last 700 Ka: Acıgöl Lake Sedıments. İstanbul Teknik Üniversitesi-Avrasya Yer Bilimleri Enstitüsü, İstanbul/Türkiye.

Altınsaçlı, S., Mezquita, F., 2008. Ostracod fauna of salt Lake Acıgöl (Acı Tuz) (Turkey). J. Nat. Hist. 42 (13), 1013–1025. https://doi.org/10.1080/00222930701851735.

Alçiçek, H., 2009. Late Miocene nonmarine sedimentation and formation of magnesites in the Acıgöl Basin, southwestern Anatolia, Turkey. Sediment. Geol. 219, 115–135. https://doi.org/10.1016/j.sedgeo.2009.05.002.

Alçiçek, M.C., Brogi, A., Capezzuoli, E., Liotta, D., Meccheri, M., 2013. Superimposed basin formation during Neogene–Quaternary extensional tectonics in SW-Anatolia (Turkey): insights from the kinematics of the Dinar fault zone. Tectonophysics 608, 713–727. https://doi.org/10.1016/j.tecto.2013.08.008.

Alçiçek, M.C., Mayda, S., Titov, V., 2013. Lower pleistocene stratigraphy of the burdur basin of SW Anatolia. Comptes Rendus Palevol 12, 1–11. https://doi.org/10.1016/j.crpv.2012.09.005.

Alçiçek, M.C., Mayda, S., Ten Veen, J.H., Boulton, S.J., Neubauer, T.A., Alçiçek, H., Tesakov, A., Saraç, G., Hakyemez, H.Y., Göktaş, F., Murray, A.M., Titov, V., Jiménez-Moreno, G., Demirel, A., Kaya, T., Halaçlar, K., Bilgin, M., Van den Hoek Ostende, L. W., 2019. Reconciling the stratigraphy and sedimentation history of the Lycian orogen-top basins, SW Anatolia. Palaeobiodivers. Palaeoenviron. https://doi.org/10.1007/s12549-019-00394-3.

Anderson, R.Y., Dean, W.E., Bradbury, J.P., Love, D., 1985. Meromictic lakes and varved lake sediments in North America. U. S. Geol. Surv. Bull. 1607, 19.

Besse, J., Courtillot, V., 2002. Apparent and true polar wander and the geometry of the geomagnetic field over the last 200 Myr. J. Geophys. Res. https://doi.org/10.1029/2000JB000050.

Beug, H.J., 2004. Leitfaden der Pollenbestimmung für Mitteleuropa und angrenzende Gebiete. Verlag Friedrich Pfeil, München, p. 542. https://doi.org/10.1016/j.revpalbo.2004.06.003.

Bloemendal, J., King, J.W., Hall, F.R., Doh, S.-J., 1992. Rock magnetism of Late Neogene and Pleistocene deep-sea sediments: relationship to sediment source, diagenetic processes, and sediment lithology. J. Geophys. Res. 97 (b4), 4361–4375. https://doi.org/10.1029/91JB03068.

Boulbes, N., Mayda, S., Titov, V., Alçiçek, M.C., 2014. Les grands mammifères du Villafranchien supérieur des travertins du Bassin de Denizli, Sud-Ouest Anatolie, Turquie (*The Late Villafranchian large mammals from the Denizli Basin travertines, Southwest Anatolia, Turkey*). L'Anthropologie 118, 44–73. https://doi.org/10.1016/j.anthro.2014.01.001.

Boulbes, N., Mayda, S., Titov, V.V., Alçiçek, C., 2014. Les grands mammifères du Villafranchien supérieur des travertins du Bassin de Denizli (Sud-Ouest Anatolie, Turquie). L'Anthropologie 118, 44–73. https://doi.org/10.1016/j.anthro.2014.01.001.

Bourlès, D.L., Raisbeck, G.M., Yiou, F., 1989. ^{10}Be and ^{9}Be in marine sediments and their potential for dating. Geochem. Cosmochim. Acta 53, 443–452. https://doi.org/10.1016/0016-7037(89)90395-5.

Chmeleff, J., von Blanckenburg, F., Kossert, K., Jakob, D., 2010. Determination of the ^{10}Be half-life by multicollector ICP-MS and liquid scintillation counting. Nucl. Instrum. Methods Phys. Res. Sect. B Beam Interact. Mater. Atoms 268, 192–199. https://doi.org/10.1016/j.nimb.2009.09.012.

Cukur, D., Krastel, S., Schmincke, H.U., Sumita, M., Tomonaga, Y., Çağatay, M.N., 2014. Water level changes in Lake Van, Turkey, during the past ca. 600 ka: climatic, volcanic and tectonic controls. J. Paleolimnol. 52, 201–214. https://doi.org/10.1007/s10933-014-9788-0.

Day, R., Fuller, M., Smith, V.A., 1977. Hysteresis properties of titanomagnetites: grain-size and compositional dependence. Phys. Earth Planet. Inter. 13, 260–267. https://doi.org/10.1016/0031-9201(77)90108-X.

Demory, F., Nowaczyk, N., Witt, A., Oberhänsli, H., 2005. High-resolution magnetostratigraphy of late quaternary sediments from Lake Baikal, Siberia: timing of intracontinental paleoclimatic responses. Glob. Planet. Chang. 46 (1–4), 167–186. https://doi.org/10.1016/j.gloplacha.2004.09.016.

Develle, A.L., Gasse, F., Vidal, L., Williamson, D., Demory, F., Van Campo, E., Ghaleb, B., Thouveny, N., 2011. A 250 ka sedimentary record from a small karstic lake in the Northern Levant (Yammouneh, Lebanon) paleoclimatic implications. Palaeogeogr. Palaeoclimatol. Palaeoecol. 305 (1-4), 10–27,. https://doi.org/10.1016/j.palaeo.2011.02.008.

Dunlop, D.J., 2002. Theory and application of the Day plot (Mrs/Ms versus Hcr/Hc) 1. Theoretical curves and tests using titanomagnetite data. J. Geophys. Res. Atmos. 107 https://doi.org/10.1029/2001JB000486, 2056, EPM 4-1-4-22.

Fowell, S.J., Hansen, B.C.S., Peck, J.A., Khosbayar, P., Ganbold, E., 2003. Mid to Late Holocene Climate Evolution of the Lake Telmen Basin, North Central Mongolia, Based on palynological Data, 59, pp. 353–363. https://doi.org/10.1016/S0033-5894(02)00020-0.

Francke, A., Wagner, B., Just, J., Leicher, N., Gromig, R., Baumgarten, H., Vogel, H., Lacey, J.H., Sadori, L., Wonik, T., Leng, M.J., Zanchetta, G., Sulpizio, R., Giaccio, B., 2016. Sedimentological processes and environmental variability at Lake Ohrid (Macedonia, Albania) between 637 ka and the present. Biogeosciences 13, 1179–1196. https://doi.org/10.5194/bg-13-1179-2016.

Gasse, F., Vidal, L., Develle, A.L., VanCampo, E., 2011. Hydrological variability in the Northern Levant: a 250 ka multiproxy record from the Yammoûneh (Lebanon) sedimentary sequence. Clim. Past 7, 1261–1284. https://doi.org/10.5194/cp-7-1261-2011.

Glenn, C.R., Kelts, K., 1991. Sedimentary rhythms in lake deposits. In: Einsele, G., Ricken, W., Seilacher, A. (Eds.), Cycles and Events in Stratigraphy. Springer-Verlag, New York, pp. 188–221.

Göktaş, F., Çakmakoğlu, A., Tari, E., Sütçü, Y.F., ve Sarikaya, H., 1989. Çivril –Çardak Arasının Jeolojisi (Geology of Çivril-Çardak region]. MTA Raporu 8701, 107s (yayınlanmamış).

Graham, I.J., Ditchburn, R.G., Whitehead, N.E., 2001. Be isotope analysis of a 0–500 ka loess–paleosol sequence from Rangitatau East, New Zealand. Quat. Int. 76–77, 29–42. https://doi.org/10.1016/S1040-6182(00)00087-2.

Helvaci, C., Alçicek, M.C., Gündoğan, I.̇, Gemici, Ü., 2013. Tectonosedimentary development and palaeoenvironmental changes in the Acıgöl shallow-perennial playa-lake basin, SW Anatolia, Turkey. Turk. J. Earth Sci. 22 (2), 173–190. https://doi.org/10.3906/yer-1112-5.

Kappelman, J., Alçiçek, M.C., Kazanci, N., Schultz, M., Özkul, M., Şen, Ş., 2008. First *Homo erectus* from Turkey and implications for migrations into temperate Eurasia. Am. J. Phys. Anthropol. 135, 110–116.

Konak, N., 2002. Geological map of Turkey in 1/500.000 scale: İzmir sheet. Min. Res. Expl. Directorate Turkey (MTA), Ankara.

Konak, N., Şenel, M., 2002. Geological map of Turkey in 1:500000 scale: Denizli sheet. Publ. Min. Res. Exp. Directorate of Turkey.

Korschinek, G., Bergmaier, A., Faestermann, T., Gerstmann, U.C., Knie, K., Rugel, G., Wallner, A., Dillmann, I., Dollinger, G., Lierse von Gostomski, C., Kossert, K., Maiti, M., Poutivtsev, M., Remmert, A., 2010. A new value for the ^{10}Be half-life by Heavy-Ion Elastic Recoil Detection and liquid scintillation counting. Nucl. Inst. Methods Phys. Res. B Beam Interact. Mater. Atoms 268 (2), 187–191. https://doi.org/10.1016/j.nimb.2009.09.020.

Kwiecien, O., Stockhecke, M., Pickarski, N., Heumann, G., Litt, T., Sturm, M., Anselmetti, F.S., Kipfer, R., Haug, G.H., 2014. Dynamics of the last four glacial terminations recorded in Lake Van. Turkey. Quat. Sci. Rev. 104, 42–52. https://doi.org/10.1016/j.quascirev.

Lebatard, A.E., Bourlès, D.L., Duringer, P., Jolivet, M., Braucher, R., Carcaillet, J., Schuster, M., Arnaud, N., Monié, P., Lihoreau, F., Likius, A., Mackaye, H.T., Vignaud, P., Brunet, M., 2008. Cosmogenic nuclide dating of Sahelanthropus tchadensis and Australopithecus bahrelghazali: mio-Pliocene hominids from Chad. Proc. Natl. Acad. Sci. 105, 3226–3231. https://doi.org/10.1073/pnas.0708015105.

Lebatard, A.E., Bourlès, D.L., Braucher, R., Arnold, M., Duringer, P., Jolivet, M., Moussa, A., Deschamps, P., Roquin, C., Carcaillet, J., Schuster, M., Lihoreau, F., Likius, A., Mackaye, H.T., Vignaud, P., Brunet, M., 2010. Application of the authigenic ^{10}Be/^{9}Be dating method to continental sediments: reconstruction of the Mio-Pleistocene sedimentary sequence in the early hominid fossiliferous areas of the northern Chad Basin. Earth Planet. Sci. Lett. 297 (1–2), 57–70. https://doi.org/10.1016/j.epsl.2010.06.003.

Lebatard, A.-E., Alçiçek, M.C., Rochette, P., Khatib, S., Vialet, A., Boulbes, N., Bourlès, D. L., Demory, F., Guipert, G., Mayda, S., Titov, V.V., Vidal, L., de Lumley, H., 2014. Dating the Homo erectus bearing travertine from Kocabaş (Denizli, Turkey) at at least 1.1 Ma. Earth Planet. Sci. Lett. 390, 8–18. https://doi.org/10.1016/j.epsl.2013.12.031.

Lisiecki, L.E., Raymo, M.E., 2005. A Pliocene-Pleistocene stack of 57 globally distributed benthic d^{18}O records. Paleoceanography 20, PA1003. https://doi.org/10.1029/2004PA001071.

Liu, Q., Roberts, A.P., Torrent, J., Horng, C.S., Larrasoaña, J.C., 2007. What do the HIRM and *S*-ratio really measure in environmental magnetism? Geochem. Geophys. Geosyst. 8, Q09011 https://doi.org/10.1029/2007GC001717.

Lowrie, W., 1990. Identification of ferromagnetic minerals in a rock by coercivity and unblocking temperature properties. Geophys. Res. Lett. 17 (2), 159–162.

Moore, P.D., Webb, J.A., Collinson, M.E., 1991. Pollen Analysis, second ed. Blackwell Scientific Publications, Oxford.
Mutlu, H., Kadir, S., Akbulut, A., 1999. Mineralogy and water chemistry of the lake Acıgöl, Denizli, Turkey. Carbonates Evaporites 14 (2), 191–199.
Novello, A., Lebatard, A.-E., Moussa, A., Barboni, D., Sylvestre, F., Bourlès, D.L., Paillès, C., Buchet, G., Decarreau, A., Duringer, P., Ghienne, J.-F., Maley, J., Mazur, J.-C., Roquin, C., Schuster, M., Vignaud, P., 2015. Diatom, phytolith, and pollen records from a $^{10}Be/^{9}Be$ dated lacustrine succession in the Chad basin: insight on the Miocene–Pliocene paleoenvironmental changes in Central Africa. Palaeogeogr. Palaeoclimatol. Palaeoecol. 430, 85–103. https://doi.org/10.1016/j.palaeo.2015.04.013.
Ogg, J.G., 2012. Geomagnetic polarity time scale. In: Gradstein, F.M., Ogg, J.G., Schmitz, M., Ogg, G. (Eds.), The Geologic Time Scale 2012. Published by Elsevier B. V., pp. 85–113. https://doi.org/10.1016/B978-0-444-59425-9.00005-6
Price, S.P., Scott, B., 1994. Fault–block rotations at the edge of a zone of continental extension: southwest Turkey. J. Struct. Geol. 16 (3), 381–392. https://doi.org/10.1016/0191-8141(94)90042-6.
Reille, M., 1992. Pollen et spores d'Europe et d'Afrique du Nord. Laboratoire de Botanique historique et Palynologie, Marseille, p. 543.
Reille, M., 1995. Pollen et spores d'Europe et d'Afrique du Nord, supplément 1. Laboratoire de Botanique historique et Palynologie, Marseille, p. 327.
Reille, M., 1998. Pollen et spores d'Europe et d'Afrique du Nord, supplément 2. Laboratoire de Botanique historique et Palynologie, Marseille, p. 530.
Roeser, P., Franz, S.O., Litt, T., 2016. Aragonite and calcite preserva- tion in sediments from Lake Iznik related to bottom lake oxygen- ation and water column depth. Sedimentology 63, 2253–2277. https://doi.org/10.1111/sed.12306.
Şenel, M., 2002. Geological map of Turkey in 1:500000 scale: Konya sheet. Mineral Res. Expl. Direct. Turkey (MTA), Ankara, Turkey.
Simon, Q., Thouveny, N., Bourlès, D.L., Nuttin, L., Hillaire-Marcel, C., St-Onge, G., 2016. Authigenic $^{10}Be/^{9}Be$ ratios and 10Be-fluxes (230Thxs-normalized) in central Baffin Bay sediments during the last glacial cycle: paleoenvironmental implications. Quat. Sci. Rev. 140, 142–162. https://doi.org/10.1016/j.quascirev.2016.03.027.
Stober, J.C., Thompson, R., 1977. Palaeomagnetic secular variation studies of Finnish lake sediment and the carriers of remanence. Earth Planet. Sci. Lett. 37 (1), 139–149. https://doi.org/10.1016/0012-821X(77)90155-8.
Šujan, M., Braucher, R., Kováč, M., Bourlès, D.L., Rybár, S., Guillou, V., Hudáčková, N., 2016. Application of the authigenic $^{10}Be/^{9}Be$ dating method to late miocene–pliocene sequences in the northern Danube basin (Pannonian basin system): confirmation of heterochronous evolution of sedimentary environments. Glob. Planet. Chang. 137, 35–53. https://doi.org/10.1016/j.gloplacha.2015.12.013.
Ten Veen, J.H., Boulton, S.J., Alçiçek, M.C., 2009. From palaeotectonics to neotectonics in the Neotethys realm: the importance of kinematic decoupling and inherited structural grain in SW Anatolia (Turkey). Tectonophysics 473, 261–281. https://doi.org/10.1016/j.tecto.2008.09.030.
Turan, N., 2002. Geological Map of Turkey in 1:500000 Scale: Ankara Sheet. Publication of Mineral Research and Explaniton Directorate of Turkey (MTA), Ankara.
Van Vugt, N., Langereis, C.G., Hilgen, F.J., 2001. Orbital forcing in Pliocene–Pleistocene Mediterranean lacustrine deposits: dominant expression of eccentricity versus precession. Palaeogeogr. Palaeoclimatol. Palaeoecol. 172 (3–4), 193–205. https://doi.org/10.1016/S0031-0182(01)00270-X.
Vermeesch, P., 2012. On the visualisation of detrital age distributions. Chem. Geol. 312–313, 190–194. https://doi.org/10.1016/j.chemgeo.2012.04.021.
Vialet, A., Guipert, G., Alçiçek, M.C., 2012. *Homo erectus* found still further west: reconstruction of the Kocabaş cranium (Denizli, Turkey). Comptes Rendus Palevol 11, 89–95.
Vialet, A., Prat, S., Wils, P., Alçiçek, M.C., 2018. The Kocabaş hominin (Denizli Basin, Turkey) at the crossroads of Eurasia. New insights from morphometric and cladistic analyses. Comptes Rendus Palevol 17, 17–32.
Zolitschka, B., Francus, P., Ojala, A.E.K., Schimmelmann, A., 2015. Varves in Lake Sediments - A Review. Quaternary Science Reviews, vol. 117. Elsevier, pp. 1–41. https://doi.org/10.1016/j.quascirev.2015.03.019.
Nishiizumi, K., Imamura, M., Caffee, M.W., Southon, J.R., Finkel, R.C., McAninch, J., 2007. Absolute calibration of ^{10}Be AMS standards. Nucl. Inst. Methods Phys. Res. B: Beam Interactions Mater. Atoms 258, 403e413. https://doi.org/10.1016/j.nimb.2007.01.297.